

COMPRESSIBLE TURBULENT CHANNEL AND PIPE FLOW: SIMILARITIES AND DIFFERENCES

Somnath Ghosh, Rainer Friedrich

Lehrstuhl für Aerodynamik,
Technische Universität München
Boltzmannstrasse 15, D-85748 Garching, Germany
Somnath.Ghosh@aer.mw.tum.de, R.Friedrich@lrz.tum.de

Holger Foyi

Lehrstuhl für Strömungsmechanik und Aerodynamisches Institut,
RWTH Aachen
Wuellnerstrasse 5a, D-52062 Aachen, Germany
H.Foyi@aia.rwth-aachen.de

ABSTRACT

Direct numerical simulation (DNS) is used to explore similarities and differences between fully-developed supersonic turbulent plane channel and axisymmetric non-swirling pipe flow bounded by isothermal walls. The comparison is based on equal friction Mach number, friction Reynolds number, Prandtl number, ratio of specific heats and viscosity exponent. The channel half width and pipe radius are chosen to define the friction Reynolds numbers.

To what extent and why mean flow quantities, second-order turbulence statistics and terms in the Reynolds stress equations coincide or diverge in both flows is investigated. The role of the fluctuating pressure in causing characteristic differences among correlations involving pressure fluctuations is identified.

INTRODUCTION

Compressible wall-bounded turbulent flows are an important element of high-speed flight. They appear both in external flows over aerospace vehicles and in engine inlets and combustors. Although compressible wall-bounded turbulence has attracted researchers since the fifties of the last century, the underlying phenomena are not understood in all respects, even today. The direct numerical simulations (DNS) of supersonic turbulent channel flow by Coleman et al. (1995) and the companion work of Huang et al. (1995) on data analysis and modelling issues contributed strongly to a better understanding of ‘compressibility’ effects in shear flows bounded by isothermal walls. Foyi et al. (2004) gave an explanation for the reduction of pressure-strain correlations in supersonic channel flow compared to incompressible isothermal channel flow by linking it to the sharp wall-normal density variations in the framework of a Green-function-based analysis of the pressure field. It is natural to ask whether analogous effects hold in compressible flows through pipes and what the similarities or differences are between channel and pipe flow.

Comparisons between incompressible turbulent channel and pipe flow have been performed earlier. However, they were focussed on mean velocity profiles, friction laws and a few higher order statistics only. Nieuwstadt & Bradshaw

(1997) used DNS data to show that the similarity fails beyond the second-order moments and offered an explanation based on a simple model. Wosnik et al. (2000) presented a theory of the mean velocity and skin friction for fully-developed turbulent channel and pipe flow including Reynolds number effects. Nickels (2004) developed a functional form for the velocity profile of turbulent wall-bounded shear flow subjected to a strong pressure gradient which is based on the concept of a universal critical Reynolds number for the sublayer.

It is our objective to identify similarities and differences between fully-developed compressible channel and pipe flow up to second-order turbulence statistics and to provide explanations for the corresponding behaviour based on an analysis of the Reynolds stress balances and the pressure field. The results may motivate work on differences and similarities of other turbulent flows, e.g. plane and axisymmetric free shear flows.

1 DETAILS OF DIRECT SIMULATIONS

The 3D Navier-Stokes equations for compressible flow of a thermally perfect gas in cylindrical (x,r,φ) - and Cartesian (x,y,z) -coordinates are the starting point of our analysis. The viscous stresses do not contain the bulk viscosity, since it has a negligible effect in the flow regimes under consideration. The dynamic viscosity is proportional to the n^{th} power of the temperature, with $n = 0.7$. Specific heats are assumed to be constant at a ratio of $\gamma = 1.4$ for air. The Prandtl number, $Pr = 0.71$, is kept constant as well. The remaining flow parameters that uniquely characterize compressible turbulent flow are the Mach and Reynolds numbers. Parameters that are most pertinent to fully-developed turbulent channel and pipe flow are the friction Reynolds and Mach numbers, viz:

$$Re_{\tau} = \bar{\rho}_w u_{\tau} l / \bar{\mu}_w = l^+, \quad M_{\tau} = u_{\tau} / \sqrt{\gamma R \bar{T}_w} \quad (1)$$

with the length scale $l = h, R$ representing the channel half width h and the pipe radius R . The mean values of the dynamic viscosity and the speed of sound are computed at constant wall temperature \bar{T}_w . The mean density at the wall, $\bar{\rho}_w$, and the wall shear stress, $\bar{\tau}_w$, are a result of the

computation. The friction velocity reads $u_\tau = \sqrt{|\bar{\tau}_w|/\bar{\rho}_w}$. We follow common practice and apply a tilde and an overbar to define Favre and Reynolds averages, and double and single dashes to specify Favre and Reynolds fluctuations, e.g. u'' , ρ' .

Uniform body forces which equal the mean pressure-gradients drive channel and pipe flow. Non-dimensionalized with inner variables these pressure-gradients are proportional to the inverse of the Reynolds number. For pipe and channel flow, we have:

$$-\bar{p}_{x,pipe}^+ = -\frac{\bar{\mu}_w}{\bar{\rho}_w u_\tau \bar{\tau}_w} \frac{d\bar{p}}{dx} \Big|_{pipe} = \frac{2}{Re_\tau} \quad (2a)$$

$$-\bar{p}_{x,ch}^+ = -\frac{\bar{\mu}_w}{\bar{\rho}_w u_\tau \bar{\tau}_w} \frac{d\bar{p}}{dx} \Big|_{ch} = \frac{1}{Re_\tau} \quad (2b)$$

We choose equal friction Reynolds and Mach numbers in our DNS with values specified in Table 1. Hence, the mean pressure-gradients differ in both flows. Bulk Reynolds and Mach numbers, defined with cross-sectionally averaged mean density and velocity are also included in Table 1.

Table 1: Flow parameters

Flow	Re_τ	M_τ	Re_m	M_m
Pipe	245	0.077	3181	1.30
Channel	246	0.078	2986	1.26

The fifth-order compact low-dissipation upwind scheme of Adams and Shariff (1996) and the compact sixth-order scheme of Lele (1992) are chosen to discretize convection and molecular transport terms of the governing equations. A classical third-order ‘low-storage’ Runge-Kutta advances the solution in time. The geometric singularity due to $1/r^3$ -terms in the equations is treated by placing no grid point on the cylinder axis (Mohseni & Colonius, 2000). Equidistant grids are chosen in streamwise and circumferential (spanwise) directions and grid-clustering is adopted in the wall-normal direction. The computational domains to simulate pipe/channel flow have sizes of $10R \times 2\pi R \times R$ and $4\pi h \times 4\pi h/3 \times 2h$, respectively. The cylindrical grid for supersonic pipe flow comprises $256 \times 91 \times 128$ points in (x,r,ϕ) -directions while the Cartesian grid for supersonic channel flow has $192 \times 151 \times 128$ points in (x,y,z) -directions.

2 MEAN FLOW VARIABLES AND SECOND ORDER TURBULENCE STATISTICS

In channel and pipe flow, the streamwise pressure-gradient has an effect on the whole flow domain, the importance of which - concerning the turbulence structure - decreases as the Reynolds number increases. This can be concluded from the linear relations for the total shear stresses in both flows which read as follows when correlations between fluctuations of viscosity and velocity gradients are neglected:

$$\frac{\bar{\mu}}{\bar{\mu}_w} \frac{d\bar{u}^+}{dy^+} - \frac{\overline{\rho u'' v''}}{\bar{\rho}_w u_\tau^2} = 1 + y^+ \bar{p}_{x,ch}^+ = 1 - \frac{y^+}{h^+}, \quad (channel) \quad (3a)$$

$$\frac{\bar{\mu}}{\bar{\mu}_w} \frac{d\bar{u}^+}{dy^+} - \frac{\overline{\rho u'' v''}}{\bar{\rho}_w u_\tau^2} = 1 + \frac{1}{2} y^+ \bar{p}_{x,p}^+ = 1 - \frac{y^+}{R^+} \quad (pipe) \quad (3b)$$

In eq. (3b) we have replaced the radial coordinate, r , by y , which is zero at the wall and is defined through $y=R-r$. Furthermore, we have substituted the radial velocity

component, setting $u_r = -v$. A comparison of viscous and Reynolds shear stresses for the flow parameters given in Table 1 is presented in Figure 1. In this and the following figures dotted/solid lines represent channel/pipe flow, respectively. All curves seem to lie on top of each other.

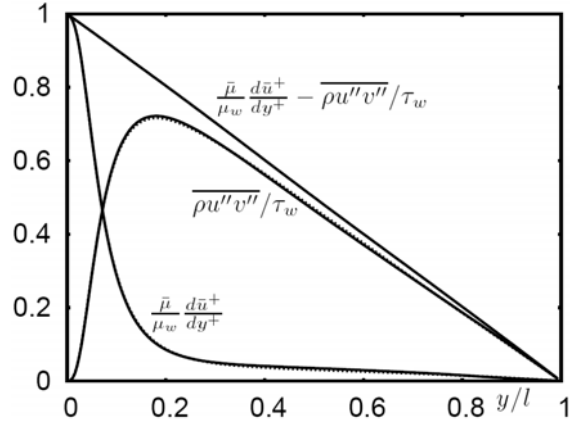


Fig. 1: Reynolds and viscous shear stress, together with total stress for channel and pipe flow, according to eqs. (2a,b).

Figure 2 shows profiles of the van Driest transformed mean velocity $\bar{u}_{VD}^+(y^+)$ for channel and pipe flow. The curves seem to collapse in the viscous sublayer. A closer look, however, reveals subtle differences even close to the wall which result from differences in the mean viscosities of channel and pipe flow, as explained below. In the fully turbulent region the channel has a flatter velocity profile than the pipe which points towards distinct differences in the integral parameters.

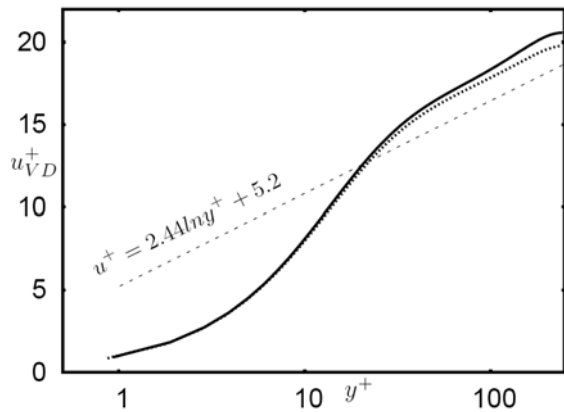


Fig. 2: Van Driest transformed mean velocity versus y^+ .

The integrated wall-normal momentum equations read for channel and pipe flow:

$$\bar{p} = \bar{p}_w - \overline{\rho v'' v''} \quad (channel) \quad (4a)$$

$$\bar{p} = \bar{p}_w - \overline{\rho v'' v''} - \int_0^{y/R} \left(\overline{\rho v'' v''} - \overline{\rho w'' w''} \right) \frac{d(y/R)}{(1-y/R)} \quad (pipe) \quad (4b)$$

They reveal an important qualitative difference between pipe and channel flow resulting from the transverse curvature term. Plots of these profiles in figure 3, show

indeed characteristic differences which seem small in this specific normalization. They amount to less than 1% of the wall pressure, but have a more sensible effect on the transverse Reynolds stresses, measured in terms of the wall shear stress, as will be seen later.

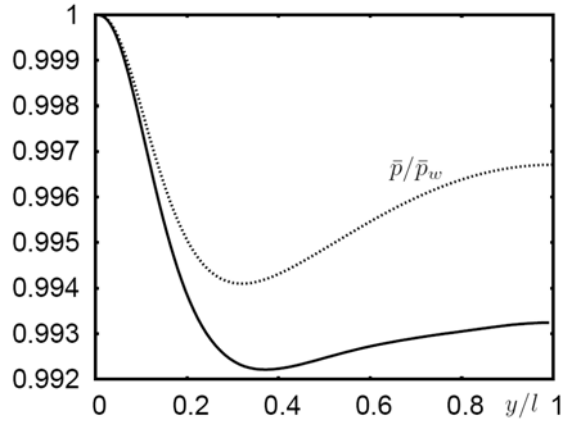


Fig. 3: Mean pressure normalized with wall pressure.

A key to the understanding of fully developed compressible turbulent channel and pipe flow lies in the rapid wall-normal changes in mean fluid properties, $\bar{\rho}$ and $\bar{\mu}(\bar{T})$, caused by viscous heating. In figure 4 we compare mean density and temperature profiles, normalized with wall values, rather than viscosity profiles. The mean viscosity behaves like the mean temperature, rises steeply in the wall layer and has a plateau in the core.

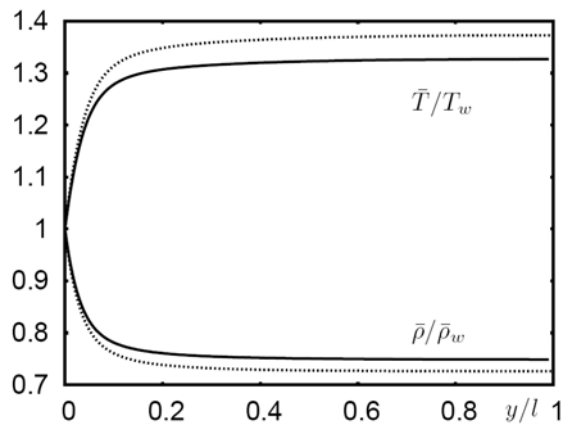


Figure 4: Mean density and temperature for channel and pipe flow, normalized with wall values.

Obviously, density and temperature differ in both flows at any distance from the wall and the question is why this is so. In order to clarify this, we study the mean internal energy equation for the pipe, integrated from the wall to a position y and normalized with reference quantities at the wall:

$$\left(1 - \frac{y^+}{R^+}\right) \left(\frac{\gamma}{Pr} \frac{\bar{\lambda}}{\bar{\lambda}_w} \frac{d\bar{T}/\bar{T}_w}{dy^+} - \frac{\overline{\rho v'' T''}}{\rho_w u_\tau T_w} \right) + \gamma B_q = -\gamma(\gamma-1)M_t^2 \int_0^{y^+} \left(1 - \frac{y^+}{R^+}\right) \left(\frac{\bar{\mu}}{\bar{\mu}_w} \left(\frac{d\bar{u}^+}{dy^+} \right)^2 + \varepsilon^+ + \dots \right) dy^+ \quad (5)$$

Again, correlations involving fluctuations of molecular transport coefficients are neglected. This equation which has to be integrated a second time to obtain the mean temperature distribution in the pipe, \bar{T}/\bar{T}_w , contains on its left-hand side the mean molecular heat flux, the turbulent heat flux and the heat flux into the wall, in terms of the non-dimensional heat flux, $B_q = q_w / (\bar{\rho}_w c_p u_\tau \bar{T}_w)$. The right-hand side comprises the integrated effects of direct and turbulent kinetic energy dissipation ($\varepsilon^+ = \varepsilon \bar{\mu}_w / \bar{\tau}_w^2$). Mean pressure-dilatation as well as pressure-dilatation correlation have been neglected, since they are known to be small up to supersonic speeds (Coleman et al., 1995, Huang et al., 1995). An equation, similar to (5) is obtained for channel flow, just by setting the brackets, $(1 - y^+/R^+)$, in (5) equal to one. Hence an obvious difference between channel and pipe flow arises from wall curvature, and this difference disappears only in the limit of very high Reynolds number R^+ . Figure 5 contains profiles of the relevant terms in eq. (22) for both flows, normalized with the wall heat fluxes. At a certain position y/h in the channel, the mean molecular and turbulent heat fluxes surpass those in the pipe at y/R . In contrast to this is the integrated direct dissipation rate everywhere in the channel lower than in the pipe, as a result of lower mean velocity gradients. The integrated turbulent dissipation rate is lower in the wall-layer of the channel, but overshoots that of the pipe in the core region.

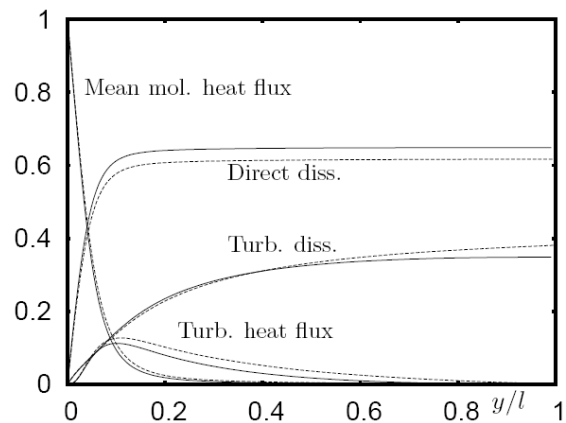


Figure 5: Profiles of the mean molecular and turbulent heat fluxes and of the integrated effects of direct and turbulent dissipation rate, normalized with the wall heat flux, for channel and pipe flow, according to eq. (5).

In figures 6-8 we present profiles of the three normal Reynolds stresses, normalized with $\bar{\tau}_w$, versus the semi-local coordinate, $y^* = y^+ \bar{\mu}_w / \bar{\mu} \sqrt{\bar{\rho} / \bar{\rho}_w}$. It is interesting to note that in the wall-layer of the pipe each of the normal Reynolds stresses collapses onto the corresponding curve for the channel. While the peak values of the streamwise and spanwise (circumferential) stresses still pretty much coincide, those of the wall-normal Reynolds stress do not. Furthermore, we observe differences between channel and pipe flow in their fully-turbulent regions for the wall-normal and spanwise stresses. An explanation for this behaviour has to start from the Reynolds stress transport equations.

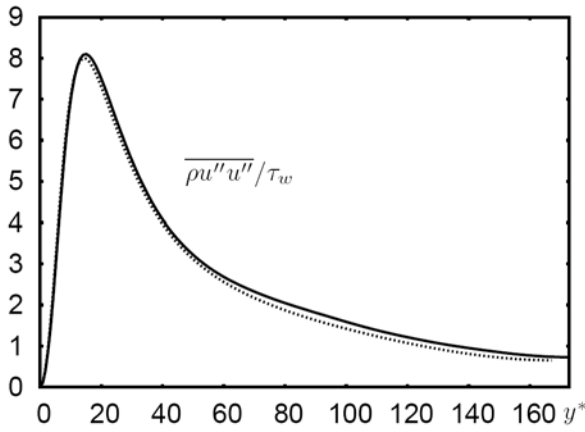


Figure 6: Streamwise Reynolds stress versus y^* .

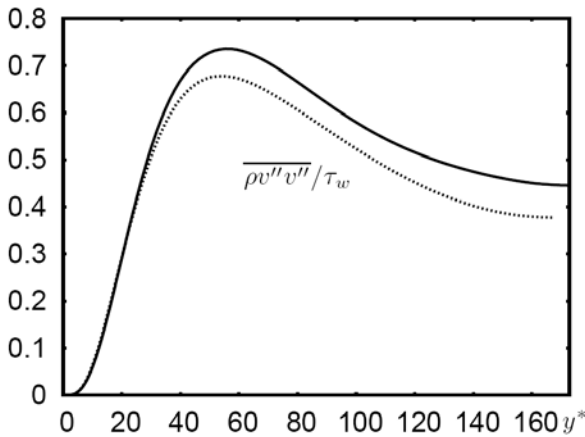


Figure 7: Wall-normal Reynolds stress versus y^* .

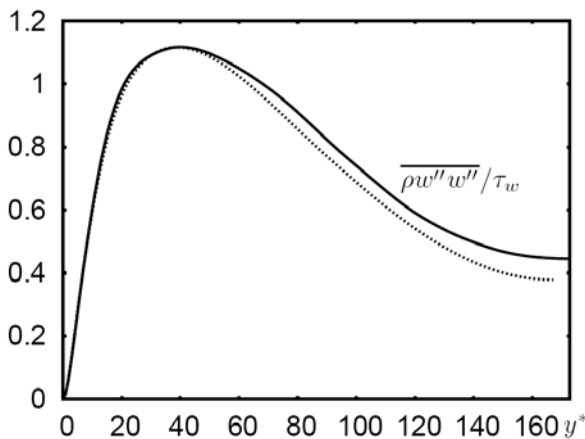


Figure 8: Spanwise (circumf.) Reynolds stress versus y^* .

Anticipating differences in the pressure-strain correlations, we present profiles of the RMS-pressure fluctuations in figure 9, normalized with the wall shear stress. The pressure fluctuations in the channel lie consistently below those for the pipe. Even the wall value is roughly 10% lower. The three components of the RMS vorticity fluctuations are plotted in figure 10, normalized with the friction velocity squared and the viscosity at wall-temperature.

Here, again, does the fully-turbulent flow in the channel core produce weaker vorticity fluctuations than that of the pipe. The opposite is true for the spanwise component ω_z' close to the wall.

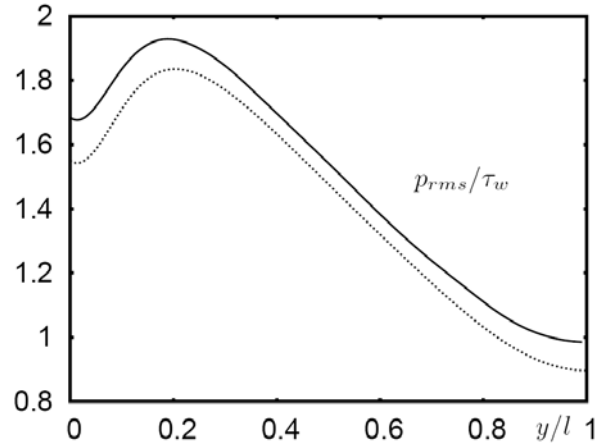


Fig. 9 : RMS pressure fluctuations normalized with the wall shear stress versus y/l , y/h .

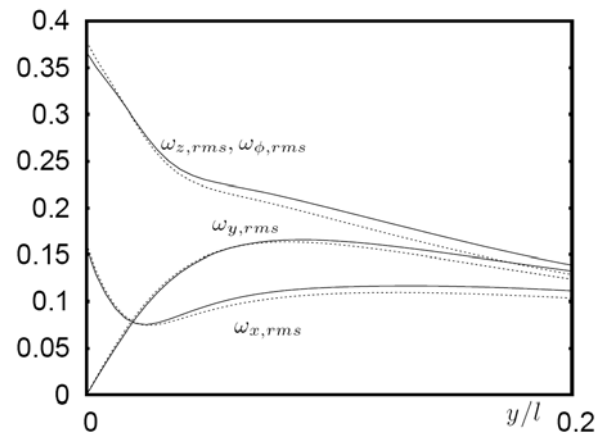


Fig. 10 : RMS vorticity fluctuations, normalized with the friction velocity squared and the wall viscosity.

3 REYNOLDS STRESS TRANSPORT

For fully-developed pipe flow the transport equation for the streamwise Reynolds stress $\overline{\rho u'' u''}$ reads:

$$0 = \underbrace{-2\overline{\rho u'' v''} \frac{d\bar{u}}{dy}}_{P_{xx}} - \underbrace{\frac{1}{(1-y/R)} \frac{d(1-y/R)\overline{\rho u'' u'' v''}}{dy}}_{TT_{xx}} + \underbrace{2p' \frac{\partial u''}{\partial x}}_{PS_{xx}} + \underbrace{\frac{2}{(1-y/R)} \frac{d(1-y/R)\overline{\tau'_{xy} u''}}{dy}}_{VD_{xx}} + \underbrace{2\overline{u''} \left(\frac{1}{(1-y/R)} \frac{d(1-y/R)\overline{\tau'_{xy}}}{dy} - \frac{\partial \bar{p}}{\partial x} \right)}_{M_{xx}} - \underbrace{2\overline{\tau'_{xx}} \frac{\partial u''}{\partial x}}_{DS_{xx}} - \underbrace{2\overline{\tau'_{xy}} \frac{\partial u''}{\partial y}}_{DS_{xx}} - \underbrace{\frac{2}{R-y} \overline{\tau'_{x\phi}} \frac{\partial u''}{\partial \phi}}_{DS_{xx}} \quad (6)$$

where the labels of the various terms have the following meaning: P_{xx} : production, TT_{xx} : turbulent transport, VD_{xx} : viscous diffusion, PS_{xx} : pressure-strain rate redistribution, DS_{xx} : turbulent dissipation rate, M_{xx} : mass-flux variation

(viscous and pressure work). The corresponding equation for channel flow is easily obtained from (6) by setting $(1 - y/R) = 1$ and $\partial/r\partial\phi = \partial/\partial z$. Comparing the equations for channel and pipe term by term one notes that there are no explicit differences. Figures 11a,b, however, reveal subtle differences among the amplitudes of the terms, when normalized with $\bar{\tau}_w^2/\bar{\mu}$, as suggested by Foysi et al. (2004). Concerning the production term, there is practically no visible difference, at least up to its peak. In the fully turbulent flow region ($y^* > 30$) the source terms P_{xx} , DS_{xx} , PS_{xx} and even the turbulent transport term TT_{xx} show differences between channel and pipe flow, in the sense that the amplitudes of these terms are consistently smaller in the channel. This is in line with the observation that the wall-normal and spanwise velocity fluctuations in the channel core are lower than in the pipe's core. Of special importance, in this context, is the fact that the pressure strain correlation in the channel is reduced compared to that in the pipe. As a consequence the wall-normal and spanwise Reynolds stresses receive less energy than the corresponding stresses in the pipe, which is indeed the case. We like to emphasize a further interesting point observed close to the wall, figure (11a), namely the fact that the viscous diffusion and dissipation terms in the channel have higher amplitudes than those in the pipe. To show that this is a physical effect, the wall-value of the viscous diffusion term can be expressed in non-dimensional form as:

$$\frac{VD_{xx}}{\bar{\tau}_w^2/\bar{\mu}} \Big|_w = \frac{d^2 u'^2 / u_\tau^2}{dy^{+2}} \Big|_w \quad (7)$$

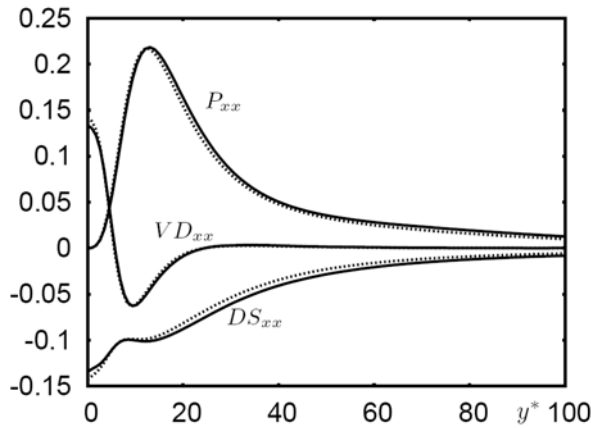


Fig. 11a: Terms of the streamwise Reynolds stress budget versus y^* . Production (P_{xx}), dissipation (DS_{xx}) and viscous diffusion (VD_{xx}).

Inspection of profiles of the non-dimensional streamwise RMS velocity fluctuations indeed reveals slightly higher curvature close to the channel wall (not shown here), and this is consistent with the higher spanwise RMS vorticity fluctuation in figure 10. In line with the near-wall effects of the streamwise Reynolds stress, we observe higher amplitudes of the pressure-diffusion and pressure-strain terms in the wall-normal Reynolds stress (figure 12), which might be physically related to subtle changes of the splatting mechanism during sweep events. The transverse curvature of the pipe might inhibit the spanwise spreading of fluid

during such an event (ramp effect), and this would then be reflected in corresponding damping effects of the other two components.

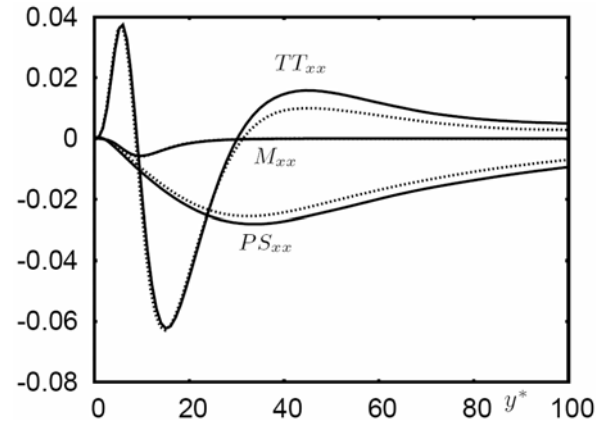


Fig. 11b: Terms of the streamwise Reynolds stress budget versus y^* . Pressure-strain correlation (PS_{xx}), turbulent transport (TT_{xx}), mass flux variation (M_{xx}).

In the fully-turbulent regions of channel and pipe, effects very similar to those discussed in the streamwise Reynolds stress balance are also found in the wall-normal, the spanwise (circumferential) and the shear stress balances, whose equations are not written down here due to lack of space.

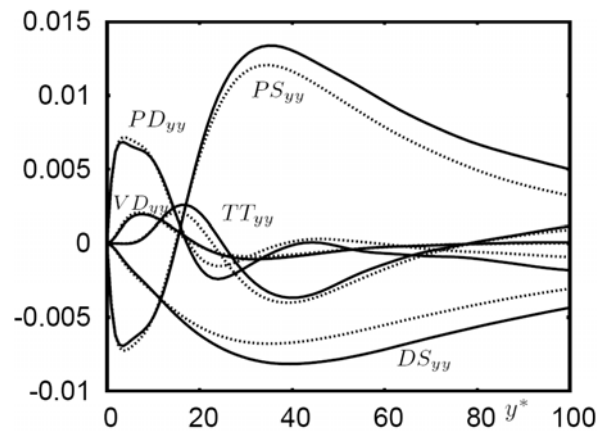


Fig. 12: Terms of the wall-normal Reynolds stress budget versus y^* . Pressure-diffusion (PD_{yy}), other symbols as in Fig. 11. Not all terms are plotted.

Profiles of the corresponding production, pressure-strain, pressure-diffusion, viscous diffusion, turbulent transport and dissipation terms are displayed in figures 12, 13 and 14. In the core region of the channel all pressure-strain terms have lower amplitudes than the corresponding terms in the pipe. Using a Green-function-based analysis of the pressure fluctuations in compressible channel flow, it has been shown by Foysi et al. (2004) that the decrease in pressure-strain correlations as the Mach number increases is linked to the decrease in mean density from the wall to the core region. Applying the same argument here, we conclude that the stronger mean density variations in the channel,

compared to those in the pipe lead to stronger reductions of the pressure-strain correlations. Concerning the lower levels of the turbulent dissipation rates in the channel core, as compared to those in the pipe, it makes sense to relate them to the lower levels of the corresponding vorticity fluctuations.

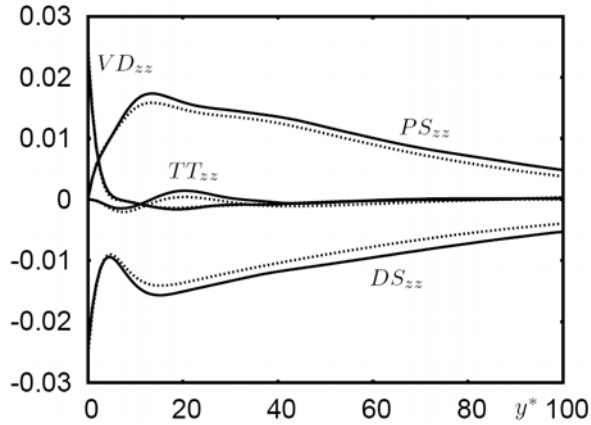


Fig. 13 : Terms of the spanwise (circumferential) Reynolds stress budget versus y^* . Not all terms are plotted for better visibility. Symbols as in figure 11.

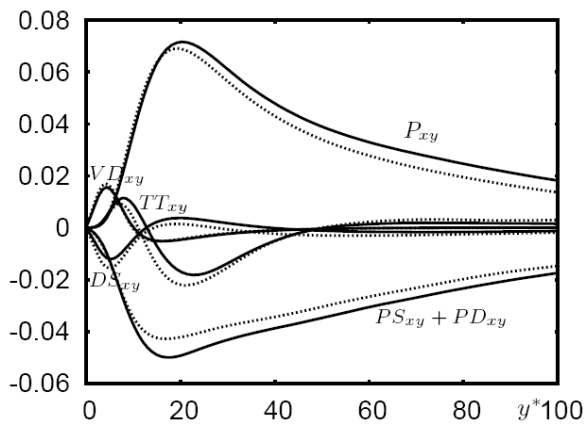


Fig. 14 : Terms of the Reynolds shear stress budget versus y^* . Not all terms are plotted for better visibility. Symbols as in figure 11.

CONCLUSIONS

A comparison of DNS data of supersonic turbulent channel and pipe flow at equal friction Reynolds and Mach numbers leads to quite similar mean viscous and Reynolds stresses in the whole flow domain and to similarities in the near-wall layer for the normal Reynolds stresses. Differences between compressible channel and pipe flow appear in the fully turbulent regions for the mean velocity and the normal Reynolds stresses. Main cause of these differences is the transverse curvature of the pipe wall which affects not only the mean pressure profile, but also lowers the mean temperature increase and mean density decrease from the wall to the centreline, and consequently raises the amount of redistributed fluctuating kinetic energy compared to that in the channel. Subtle, presumably

transverse curvature effects are also observed in wall proximity for the viscous diffusion and dissipation rates of the streamwise Reynolds stress, the pressure-diffusion and pressure-strain rates of the wall normal stress, the dissipation and viscous diffusion rate of the Reynolds shear stress and the circumferential RMS-vorticity component. When a sweep event carries high-speed fluid to the pipe wall, like an impinging jet, and transfers energy to the three velocity components, transverse curvature might act like a ramp and inhibit the spreading of fluid in circumferential direction, causing the observed effects.

ACKNOWLEDGMENTS

The first author is grateful to the German Research Association (DFG) for financial support of this work under grant number FR 478/24-1.

REFERENCES

Adams, N.A. and Shariff, K., 1996, "A high-resolution hybrid compact ENO-scheme for shock-turbulence interaction problems", *J. Comp. Phys.*, Vol. 27, pp. 27-51.
 Coleman, G.N., Kim, J. and Moser, R.D., 1995, "A numerical study of turbulent supersonic isothermal-wall channel flow", *J. Fluid Mech.*, Vol. 305, pp. 159-183.
 Foyi, H., Sarkar, S. and Friedrich, R., 2004, "Compressibility effects and turbulence scalings in supersonic channel flow", *J. Fluid Mech.*, Vol. 509, pp. 207-216.
 Huang, P.G., Coleman, G.N. and Bradshaw, P., 1995, "Compressible turbulent channel flows: DNS results and modelling", *J. Fluid Mech.*, Vol. 305, pp. 185-218.
 Lele, S.K., 1992, "Compact finite difference schemes with spectral-like resolution", *J. Comp. Physics*, Vol. 103, pp. 16-42.
 Mohseni, K. and Colonius, T., 2000, "Numerical treatment of polar coordinate singularities", *J. Comp. Physics*, Vol. 157, pp. 787-795.
 Nickels, T.B., 2004, "Inner scaling for wall-bounded flows subject to large pressure gradients", *J. Fluid Mech.*, Vol. 521, pp. 217-239.
 Nieuwstadt, F.T.M. and Bradshaw, P., 1997, "Similarities and differences of turbulent boundary-layer, pipe and channel flow". – In: *Boundary-layer separation in aircraft aerodynamics*, R.A.W.M. Henkes & P.G. Bakker, ed., Delft University Press, pp. 15-22.
 Wosnik, M., Castillo, L. and George, W.K., 2000, "A theory for turbulent pipe and channel flows", *J. Fluid Mech.*, Vol. 421, pp. 115-145.